Microplastic fouling: A gap in knowledge and a research imperative to improve their study by infrared characterization spectroscopy

Mikaël Kedzierski, Maialen Palazot, Lata Soccalingame, Maria Luiza Pedrotti, Stéphane Bruzaud

▶ **To cite this version:**

Mikaël Kedzierski, Maialen Palazot, Lata Soccalingame, Maria Luiza Pedrotti, Stéphane Bruzaud. Microplastic fouling: A gap in knowledge and a research imperative to improve their study by infrared characterization spectroscopy. Marine Pollution Bulletin, 2022, 185, pp.114306. ⟨10.1016/j.marpolbul.2022.114306⟩. ⟨hal-04007889⟩

HAL Id: hal-04007889

https://hal.science/hal-04007889v1

Submitted on 24 Jul 2025

HAL is a multi-disciplinary open access archive for the deposit and dissemination of scientific research documents, whether they are published or not. The documents may come from teaching and research institutions in France or abroad, or from public or private research centers.

L'archive ouverte pluridisciplinaire **HAL**, est destinée au dépôt et à la diffusion de documents scientifiques de niveau recherche, publiés ou non, émanant des établissements d'enseignement et de recherche français ou étrangers, des laboratoires publics ou privés.

Distributed under a Creative Commons CC BY 4.0 - Attribution - International License

Version of Record: https://www.sciencedirect.com/science/article/pii/S0025326X22009882
Manuscript_c3ab7f39ca0951a0e83e912b76a9d68e

Microplastic fouling: a gap in knowledge and a research imperative to improve their study by infrared characterization spectroscopy

Mikaël Kedzierski*[a], Maialen Palazot[a], Lata Soccalingame[a], Maria Luiza Pedrotti[b], Stéphane Bruzaud[a]

[a]Université Bretagne Sud, UMR CNRS 6027, IRDL, F-56100 Lorient, France

[b]Sorbonne Universités, UMR CNRS 7093, LOV, F-06230 Villefranche sur mer, France

Corresponding author

*E-mail: mikael.kedzierski@univ-ubs.fr

HIGHLIGHTS

- Spectra of weathered microplastics have shown new bands
- This spectral variability was mainly related to only three processes: chemical ageing, organic and inorganic fouling
- Two new polymer indices able to monitor the intensity of (bio)fouling were proposed

GRAPHICAL ABSTRACT

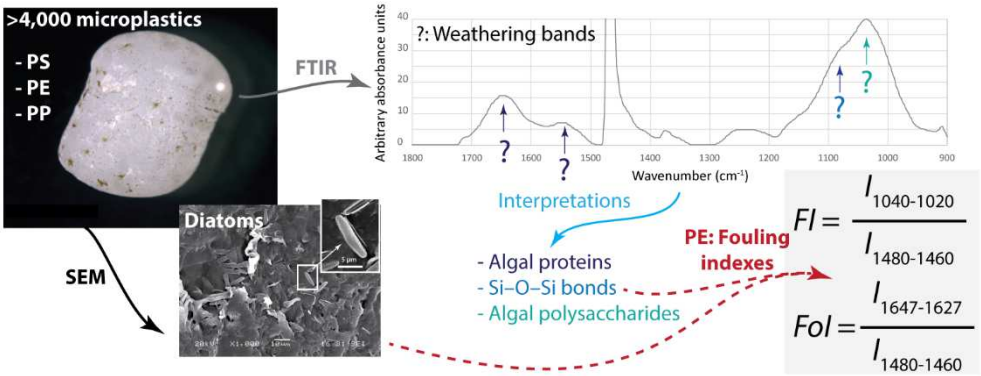

ABSTRACT

The marine weathering of microplastics is spectrally characterized by the appearance of new bands that disturb our understanding of the information carried by the spectra. Yet, no

© 2022 published by Elsevier. This manuscript is made available under the Elsevier user license
https://www.elsevier.com/open-access/userlicense/1.0/

explanation has been provided on the chemical origin of these new bands. Thus, the main objective of this work was to identify the origins of these additional bands. To this end, 4,042 spectra of poly(styrene), poly(ethylene) and poly(propylene) microplastics collected in the Mediterranean Sea, were analysed using principal component analysis. The results showed that the spectral variability was mainly related to only three processes: chemical ageing, organic and inorganic fouling. These processes probably differ from one polymer family to another due to surface affinities. This work has also led to the proposal of two new polymer indices that could be used to monitor the intensity of (bio)fouling. Finally, the development of advanced analyses could also provide information on the nature of the plastisphere.

Keywords

Microplastic, FTIR spectra, Fouling, Plastisphere, Indices

1. Introduction

In the last few years, plastic pollution has become a major environmental and health problem (Avio et al., 2017). This pollution, present from remote and uninhabited polar lands to the heights of Mount Everest, is now considered ubiquitous (Cózar et al., 2017; Lacerda et al., 2019; Napper et al., 2020).

Among the parameters studied to describe microplastic (MP) pollution, the chemical nature of the particles is of paramount importance (Gewert et al., 2017; Imhof et al., 2017; Kedzierski et al., 2022; Wang et al., 2017). Different methods such as pyrolysis-gas chromatography in combination with mass spectrometry (GC/MS) (Doyen et al., 2019; Primpke et al., 2020; Scherer et al., 2020), Raman (Dehaut et al., 2016; Long et al., 2019; Prata et al., 2019) or Infrared (IR) spectroscopy (Huo et al., 2022; Kedzierski et al., 2022; Scherer et al., 2020; Wakkaf et al., 2022), have proven their effectiveness in determining the chemical nature of

MP. Among them, Fourier transform infrared spectroscopy (FTIR) is one of the most widely used.

The appearance of additional bands is part of the classical modifications observed on an FTIR spectrum during the chemical ageing of a polymer (Andrady, 2017, 2011). To assess the level of degradation (mainly due to oxidation by solar UV radiation) by infrared spectroscopy, markers such as carbonyl index (CI) and hydroxyl index (HI) are commonly calculated from these new bands (Julienne et al., 2019). It is commonly accepted that the CI of poly(ethylene) (PE) or poly(propylene) (PP) is correlated in a controlled environment (e.g. climatic chamber) to the level of chemical ageing. This link also exists in air ageing experiments and, to a lesser extent, in aquatic environments (Andrady, 2017, 2011; Zhang et al., 2021).

However, in the marine environment, the appearance of new bands, in particular between 1800 and 1500 cm^{-1} and between 1200 and 800 cm^{-1}, disturb the understanding of the information carried by the spectra (Fernández-González et al., 2021; Kedzierski et al., 2019a; Morgado et al., 2021; Syranidou et al., 2017). In addition to disrupting CI and HI calculations, these new bands can lead to errors when spectra of weathered polymers are compared in an automated way with reference databases of virgin polymers (Fernández-González et al., 2021). These new bands are generally ignored and few explanation has yet been provided on their origin (Battulga et al., 2022).

Thus, the main objective of this work was to identify these additional bands and their origins. Then, based on this new knowledge, different potential applications for the survey of the plastiphere was proposed.

2. Materials and methods

2.1. Sample collection

Microplastic samples were collected in the Mediterranean Sea waters during the Tara Expedition which was conducted between June and November 2014 (Kedzierski et al., 2019b). Sampling was conducted using a 4.4 m long manta net (mesh size: 333 µm; net opening: 16 x 60 cm), in 124 sites which were selected based on ocean colour satellite images supplied by ACRI-ST and analysed with the Mercator circulation model. Metadata such as geographical coordinates or date of sampling are available at Zenodo Data Publisher (DOI/10.5281/zenodo.6551501.svg). At each site, the manta net was towed on the sea surface for ca. 60 min behind the boat at an average speed of 2.5 knots, enabling thus the filtration of around 507 m^3 of seawater surface.

2.2. Laboratory preparations

In the laboratory, the samples were transferred into Petri dishes. Floating plastic debris were carefully removed from other components to separate plastic particles, zooplankton and organic tissues. This process was done using a light box and a dissecting stereomicroscope to observe the sample content under high light contrast and each sample was double-checked to ensure the removal of all the smallest and/or transparent plastic particles. Thus, MP were rinsed with water, but had not undergone a digestion process. The Petri dishes containing the microplastics were dried at 50 °C for 24 h in an oven.

From 75,000 plastic items identified, a total of 15,654 particles, larger than 315 µm from 55 selected sites, were wet sieved by size class (]5-2 mm],]2-1 mm],]1-0.5 mm],]0.5-0.315 mm]). Then, they were transferred to 96-well microplates and named with a unique identifier at the Institut de Recherche Dupuy de Lôme (IRDL, Lorient, France) (Kedzierski et al., 2019b). The MP were then stored at room temperature and hygrometry.

2.3. Fourier-transform infrared spectroscopy (FTIR)

The particles spectra were acquired using an Attenuated Total Reflection Fourier Transform Infrared spectrometer (ATR-FTIR Vertex70v, Bruker). All spectra were recorded in absorbance mode in the 4,000-600 cm^{-1} region with a resolution of 4 cm^{-1} and 16 scans. Each piece of plastic was placed onto the germanium cristal (ATR Golden Gate; beam penetration at 1000 cm^{-1}: 0.66 µm), and one side per microplastic was acquired. After each analysis, the sample holder was cleaned with ethanol. The sample chamber was also cleaned out with a vacuum cleaner after every sixty analyses.

2.4. Determination of the chemical nature

FTIR spectra had already been analysed in previous studies, using the POSEIDON (Plastic pOllutionS ExtractIon, DetectiOn and aNalysis) software which is free and open source software (Kedzierski et al., 2022, 2019a, 2019b). This software was developed in the R i386 3.1.2 environment (The R Core Team, 2019).

Two pre-processing steps were performed: baseline correction, followed by spectrum normalisation (Kedzierski et al., 2019a; Liland, 2015). The machine learning process was carried out using *k*-nearest neighbour classification (Ripley, 1996; Venables et al., 2002). The learning database consisted of 969 spectra of MP and other particles (natural organic materials) collected during the 2014 Tara scientific campaign. During the identification step, if all *k*-nearest neighbours belonged to the same category, the spectrum was directly identified; otherwise the category of the spectrum was determined according to the nearest category among the *k*-nearest neighbours. If it was not possible to obtain more than two neighbours belonging to the same category, then the spectrum was automatically classified as "unknown". In order to test the accuracy of the final classification, a two-step checking was carried out involving a hierarchical cluster analysis and a principal component analysis. Then, the average spectrum of each generated subcluster was calculated and checked. If the average

spectrum of a subcluster did not match the cluster, the spectrum or group of spectra was manually identified and, possibly, reassigned to another class.

Thus, the chemical nature of 4,723 spectra was analysed by POSEIDON and among them, 131 spectra of poly(styrene) (PS), 2851 of poly(ethylene) (PE) and 1042 of poly(propylene) (PP) were identified (Kedzierski et al., 2022, 2019a).

2.5. Statistical analysis

The principal component analysis (PCA, variance-covariance matrix) was performed using PAST software (Hammer et al., 2001). The scores obtained for each of the spectra were then corrected so that the origin of the factorial map (0,0) corresponded to the spectrum of the virgin reference polymer.

Parametric correlation coefficient between main bands was also calculated with PAST software using Pearsons's test (Hammer et al., 2001).

2.6. Scanning Electron Microscope

Plastic surface imaging was performed by using a Scanning Electron Microscope (SEM; JEOL 6460-LV) at 20 kV in secondary electrons image (SEI). The chemical analysis was carried out using backscattered electron images (BSE) coupled with Energy Dispersive X-ray spectroscopy (EDS; Oxford Instrument X-ACT SATW 10mm2) at 20 kV.

2.7. Reference spectra

FTIR spectra data bank of different laboratory objects has been established. Among the spectra, those of PS, PE and PP were selected to be used as reference (non-aged polymer) (Primpke et al., 2018). These reference spectra were typical of what was described in the literature for these kinds of polymers (Lobo and Bonilla, 2003; Schröder et al., 1989). In order to safely identify spectral markers linked to potential bio and organic fouling, different spectra

were acquired and compared with literature. First, the spectrum of an alga (*Ascophyllum sp.*) collected at Kernevel harbor (GPS coordinates: 47.7173, −3.3666; France) located in the Bay of Lorient was obtained and used as a proxy. It is important to note that although derived from a macroalgal sample, the spectrum showed the main bands described for microalgae (Dean et al., 2010; Murdock and Wetzel, 2009; Quilès et al., 2010; Schmitt et al., 1995). It is for example the case of diatoms which are quite classical microalgae in the biofouling process of microplastics (Amaral-Zettler et al., 2020). It is therefore possible to use this algal spectrum as a proxy for biofouling.

Sedimentation in the Mediterranean Sea is essentially detrital with inputs of clay minerals, calcite, quartz and feldspar (Tribble and Wilkens, 1999). Among these particles suspended in the aquatic environment, quartz and clay particles can adhere to the surface of microplastics (Meng et al.,2021, Kowalski et al, 2016). A preliminary comparison between the spectra of quartz and clay particles revealed bands similar to some of the additional bands visible in the spectra of microplastics collected during the expedition. Consequently, as the mineralogical composition on the surface of microplastics is probably different from that of seawater, we chose to rely on reference spectra. Thus, spectra of quartz and clay (Talc) were extracted from the RRUFF™ Project database (https://rruff.info/) (Lafuente et al., 2015). These two spectra were combined to simulate an inorganic fouling consisting of a mixture of clay and quartz. Thus, the synthetic spectrum obtained presented bands characteristic bands of both clay and quartz.

Three spectra of MP among those collected during the 2014 campaign in the Mediterranean Sea were selected for the particularly high intensity of the additional bands. The purpose of these spectra was to illustrate the appearance of new bands in the most readable way possible. These spectra were: TM0101A11 (poly(styrene)), TM0079B9 (poly(ethylene)), and TM0075E10 (poly(propylene)). Another sample named TM0048A3 (poly(ethylene)) was also

selected to illustrate the specific aspect of the organic fouling. These spectra were named in this publication after the nomenclature developed during this campaign (Kedzierski et al., 2019b).

Through the PCA loadings, the spectrum scores were then calculated and the samples projected into the factorial maps of the Tara samples**.**

3. Results and discussion

3.1. Spectral markers of talc, quartz, and algae FTIR spectra

The spectrum of talc was characterized by bands caused by O-H stretching that occurs at 3677 cm^{-1} (Fig. 1) (Ramamoorthy et al., 2021; Schroeder, 2002; Yi et al., 2019). The tetrahedral sheet resulted in a sharp band at 1003 cm^{-1} (Ramamoorthy et al., 2021; Schroeder, 2002). Finally, two assignments prevailed in the literature of the band located at 665 cm^{-1}: the stretching vibration of Si–O–Mg (Ramamoorthy et al., 2021; Yi et al., 2019) or the libration modes of the Mg-OH in talc end-member (Dokmai et al., 2021; Schroeder, 2002). With regard to the presence of quartz, the Si–O–Si bonds resulted in bands at 1163 cm^{-1} and 1070 cm^{-1} (Anbalagan et al., 2010). The latter was partially masked by the band at 1003 cm^{-1} of talc. The stretching of Si–O bonds was also responsible for the band at 1070 cm^{-1}, but also for the band at 798 cm^{-1} (Anbalagan et al., 2010).

Concerning the spectrum of the algae (*Ascophyllum sp*.), the broad band between 3650 and ca. 3000 cm^{-1} could be attributed to both O–H and N–H stretching vibrations owing to the presence of water and proteins (Murdock and Wetzel, 2009; Schmitt et al., 1995). Bands caused by the stretching of $–CH_3$ (2968 cm^{-1}), $–CH_2$ (2923 cm^{-1}), $–CH_2$ and $–CH_3$ (2861 cm^{-1}), and related to the presence of membrane lipids in algae, were also observed (Giordano et al., 2001; Murdock and Wetzel, 2009; Quilès et al., 2010; Schmitt et al., 1995). The ester C=O stretching of membrane phospholipids gave rise to a small band around 1740 cm^{-1} (Dean

et al., 2010; Murdock and Wetzel, 2009; Quilès et al., 2010). This band could be interesting to study more precisely in the future as it could be associated with the metabolism of microorganisms on the surface of microplastics (Battulga et al., 2022). Algal proteins show up as several bands attributed to the peptide C=O stretching mode (amide I, 1637 cm^{-1}), N–H scissoring (amide II, 1541 cm^{-1}), $–CH_2$ and $–CH_3$ stretching (1456 cm^{-1}),$–CH_2$ and $–CH_3$ scissoring and C–O stretching (1396 cm^{-1}), and finally to P=O stretching (1225 cm^{-1}) (Dean et al., 2010; Giordano et al., 2001; Murdock and Wetzel, 2009). The stretching of C–O–C bonds from polysaccharides resulted in a broad band located between 1200 and 950 cm^{-1}, whose maximum intensity was observed ca. 1045 cm^{-1} (Dean et al., 2010; Murdock and Wetzel, 2009). Its large intensity should partially be due to a strong overlap with silicate related bands (Giordano et al., 2001; Stehfest et al., 2005). This is the case, for example, with diatoms whose cell wall is composed of silica and whose spectrum features an intense band located around 1075-1060 cm^{-1} (Murdock and Wetzel, 2009). This can be confused with a fouling mixing both organic and inorganic fouling.

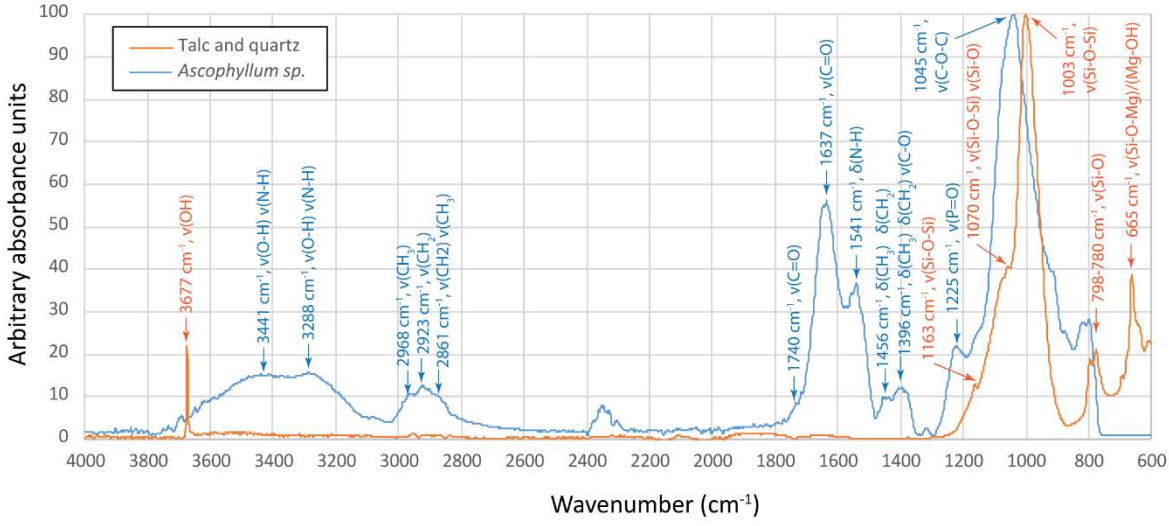

Fig. 1. Spectral markers arising from both organic and inorganic fouling of microplastics.

3.2. Identification of spectral markers occurring during ageing in the Mediterranean Sea through three samples

3.2.1. Poly(styrene)

The spectrum of the PS reference was characterized by bands associated with a mono-substituted aromatic compound (Fig. 2.a) (Lobo and Bonilla, 2003; Socrates, 2004). Normal aromatic absorption was characterized by strong bands at 3062 and 3027 cm^{-1}, corresponding to =C–H stretching, and bands at approximately 1604, 1495 and 1454 cm^{-1} related to aromatic ring stretching vibrations. Very strong bands at 755 and 698 cm^{-1} corresponded to C–H out-of-plane vibration and a ring out-of-plane deformation, respectively. The C–H stretching vibration of the aliphatic group was highlighted by bands at 2926 and 2850 cm^{-1}. The other bands, between 1400 to 800 cm^{-1}, correspond to the typical positions of the bands of aliphatic C-H deformation vibrations.

The formation of hydroxyl bonds was a characteristic of chemical ageing of the polymer. In the case of the spectrum of TM0101A11, the appearance of these bonds resulted in the increase of a very broad band between 3600 and 3000 cm^{-1}, clearly visible in the spectrum of PS aged at sea (Andrady and Pegram, 1991; Mailhot and Gardette, 1992). Then, a broad band between 1800 and 1700 cm^{-1} was clearly visible. This broad band had different maxima and shoulders at 1780, 1733, 1720 and 1709 cm^{-1}. These bands correspond to the carboxyl groups, esters and gamma-lactones of different degradation products (e.g. acetic acid, benzoic acid, carboxylic acid) formed when exposed to UV (Hüffer et al., 2018; Mailhot and Gardette, 1992). Finally, a broad band centered at approximately 1640 cm^{-1} (C=C or C=O groups) could be highlighted in the microplastic spectra (Fernández-González et al., 2021).

3.2.2. Poly(ethylene)

Chemically, poly(ethylene) can be assimilated to a long chain of methylene groups with two terminal methyl groups (Lobo and Bonilla, 2003; Socrates, 2004). Consequently, the FTIR spectrum of the PE reference was very simple (Fig. 2.b). Two very strong bands caused by

stretching vibrations show up on the spectrum at 2916 (ν_{asym} –CH_2) and 2848 cm^{-1} (ν_{sym} –CH_2). Bending modes of –CH_2 groups appeared as two doublets. The first one, assigned to –CH_2 scissoring, was located at 1471 and 1463 cm^{-1}, and the second one, to –CH_2 rocking, at 730 and 720 cm^{-1}. In the particular case of a PE exhibiting a significant branching level, two additional weak bands, typical of low-density poly(ethylene) (LDPE), could be observed at 1376 and 1363 cm^{-1}.

The changes observed in PE microplastic (TM0079B9) were relatively typical (Fernández-González et al., 2021). First, a broad band corresponding to the hydroxyl groups appeared between 3600 and 3200 cm^{-1}. However, this band was rather weak. Between 1800 and 1600 cm^{-1}, different bands related to chemical ageing were assessed and could be related to peresters or free carboxylic acids (1772 cm^{-1}), peracids (1749 cm^{-1}), aldehydes (1734 cm^{-1}), carboxylic acids (1716 cm^{-1}), γ–ketoacids and acid group (1749 cm^{-1}), and ketones (1683 cm^{-1}) (Fernández-González et al., 2021; Yagoubi et al., 2015).

3.2.3. Poly(propylene)

The FTIR spectra of the PP reference featured strong bands at 2952 and 2920 cm^{-1} due to –CH_3 stretching (symmetric and asymmetric) on the one hand, and to –CH_2 stretching (*sym* and *asym*) on the other hand (Fig. 2.c) (Chércoles Asensio et al., 2009; Socrates, 2004). Bands of medium intensity were then observed at 2870 and 2841 cm^{-1}. These bands were equally associated with –CH_3 and –CH_2 symmetric and asymmetric stretching. Medium intensity bands at 1458 and 1378 cm^{-1} were respectively associated with –CH_2 and –CH_3 scissoring. –CH_3 rocking and C–C backbone stretching were located at 1169 and 975 cm^{-1}. –CH_3 rocking and –CH_2 wagging could be seen at 1001 cm^{-1}. Finally, three other bands could be identified at 901 and 840 cm^{-1}(–CH_2 rocking) and 809 cm^{-1} (stretching of the C–C backbone).

249 The ageing of PP leads to the appearance of ageing bands similar to those observed for PE
250 (Fernández-González et al., 2021). Thus, the hydroxyl bands were found between 3600 and
251 3200 cm^{-1}. They were clearly visible in the spectrum of the microplastic (TM0075E10), but
252 partially hidden by the background. Finally, a serie of carbonyl bands can be observed
253 between 1800 and 1680 cm^{-1}. Their assignments were given in the PE previous section.

254

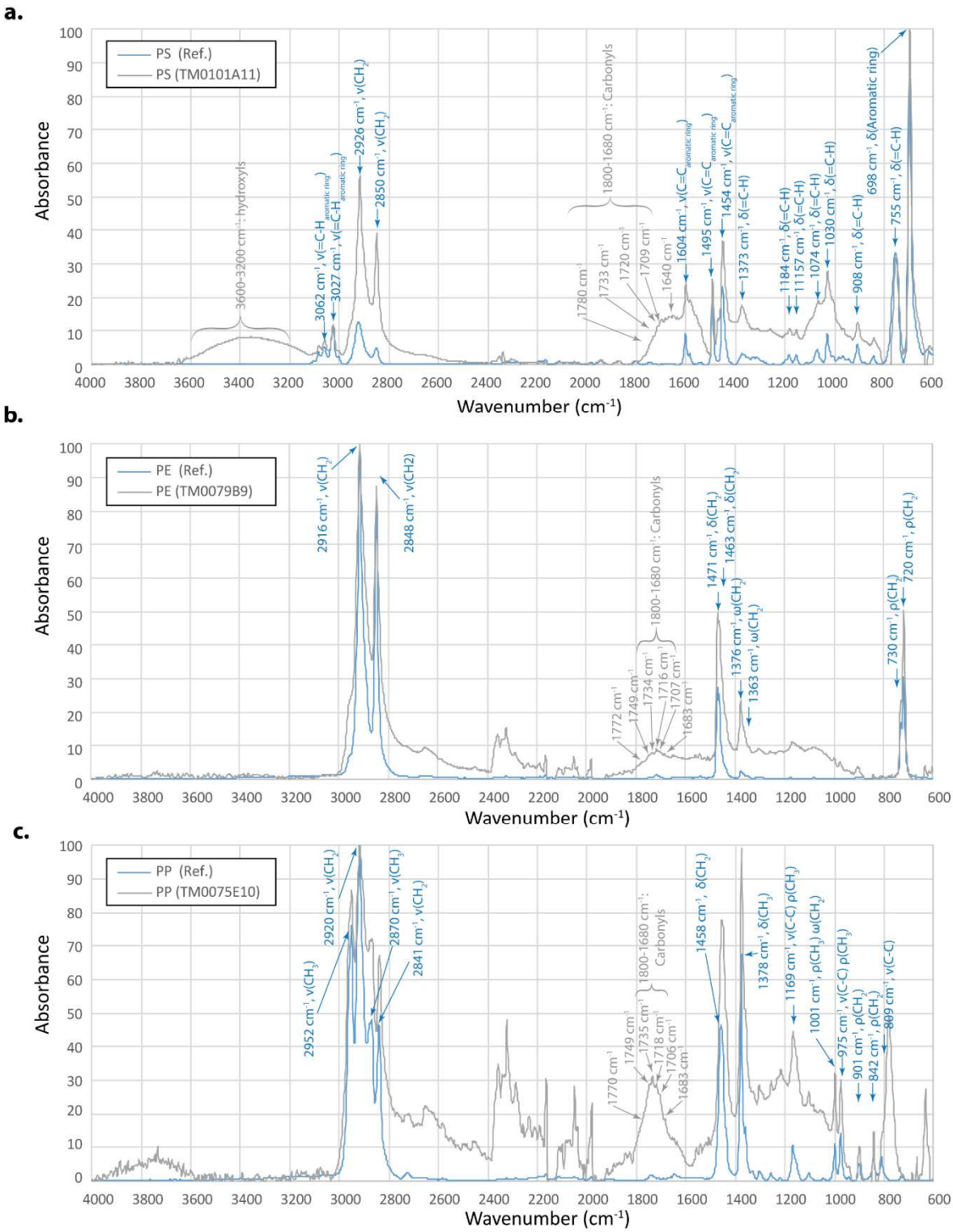

Fig. 2. Spectra of reference polymers (pristine and selected from the Tara mission data set). a. PS: poly(styrene). b. PE: Poly(ethylene). c. PP: poly(propylene).

3.3. Spectral variability of PS, PE and PP microplastics collected in the Mediterranean Sea

260 The first three PCA loadings of the PS, PE and PP spectra are presented in Fig. 3. Their
261 analysis allowed to identify, for each principal component (PC), the wavenumbers with the
262 most variance.

263 For PS, the first component PC1 accounted for 46.3% of the total variance (Fig. 3.a). Through
264 loadings analysis, this PC1 describes first the growth of bands corresponding to biotic and
265 abiotic fouling. Thus, it was necessary to note the significant weight given to the wave
266 numbers corresponding to the bands centered at 1045 and at 1003 cm^{-1}. The second
267 component (18.5%) was characterized by the significant weight of the band at 1003 cm^{-1}
268 (inorganic fouling) and to a lesser extent of the bands between 1750-1700 cm^{-1} (chemical
269 ageing). Finally, PC3 (10.9%) was less relevant than the two previous ones. The loadings of
270 PC1 and PC2 were therefore further analyzed for the PCA of PS. A high value on the PC1
271 axis indicated significant organic or inorganic fouling. A high value on the PC2 axis indicated
272 significant chemical ageing, while a low value on this axis indicated significant inorganic
273 fouling. The projection of the reference samples on the factorial map confirmed this analysis.

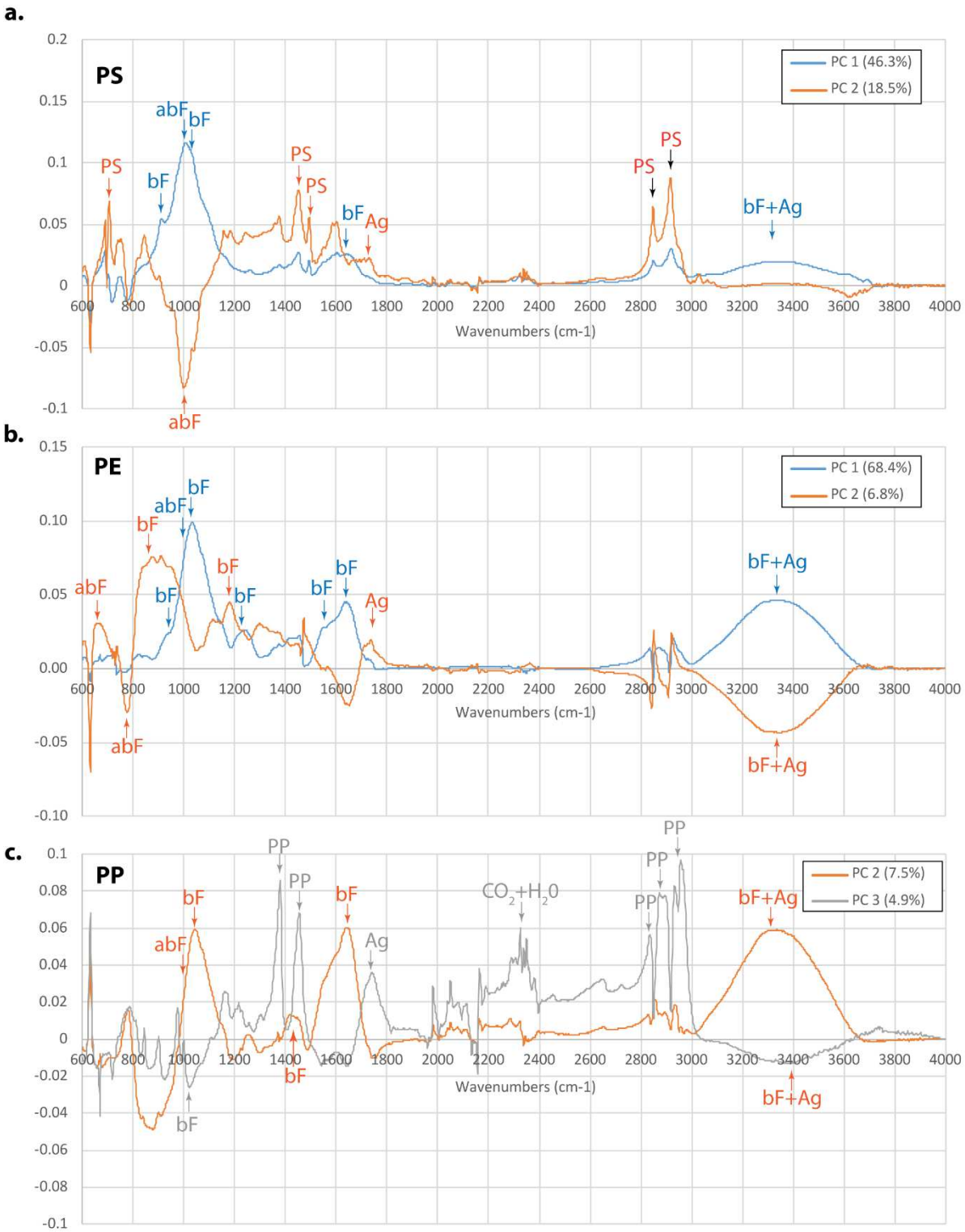

274

275 Fig. 3. Principal Component Analysis (PCA) loadings of the poly(styrene) (PS),
276 poly(ethylene) (PE) and poly(propylene) (PP). The components chosen for these PCA allow
277 to highlight the different types of weathering occurring in the natural environment. a. PC1

(68.4%) and PC2 (6.8%) were selected for PS. b. PC1 (68.4%) and PC2 (6.8%) were selected for PS. c. PC2 (7.5%) and PC3 (4.9%) were selected for PP. See explanation in the text.

For PE, PC1 accounted for 68.4% of the total variance and, as for PS, highlighted the bands related to fouling (Fig. 3.b). Thus, a high value on the x-axis (PC1) indicated intense fouling. PC2 (6.8%) was less informative because of the highlighting of the bands between 1000 and 800 cm^{-1}. PC3 was preferred because it allowed to highlight both information in terms of fouling, and chemical ageing. Thus, the higher the score, the greater ageing of the polymer, and in contrast, the lower y-axis value, the greater fouling of the polymer. This distribution was confirmed by the projection of the reference samples.

Finally, for PP, PC1 (70.0%) reflected baseline variations in the FTIR spectra (Fig. 3.c). It will therefore not be retained for the analysis. The PC2 (7.5%) characterized the state of fouling. Thus, spectra with large bands related to fouling had a high value on this axis. PC3 (4.9%) highlighted samples with significant chemical ageing, fouling, but also bands related to atmospheric CO_2 and H_2O. Thus, a high value on the x-axis (PC2) indicated significant fouling. A high value on the y-axis (PC3) indicated a high degree of chemical ageing. On the contrary, a value close to 0 reflects organic fouling. The projection of the reference samples also confirmed this interpretation.

The PS spectra were spread on the factorial map following a trifid pattern (Fig. 4.a). Most of the spectra were clustered in a zone labelled ω. The average spectrum of this zone was characterized by additional bands of moderate intensity between 1700-1500 and 1200-1000 cm^{-1}. These bands could be attributed to biofouling. Beyond the ω zone, three patterns could be identified. These patterns reflected progressive modifications of the spectra according to particular bands. The α pattern was characterized by spectra showing increasingly intense carbonyl bands (between 1800 and 1700 cm^{-1}). However, it should be noticed that these bands were not very differentiated on the spectra, probably because of the superposition in the same

303 spectral area of these bands associated with chemical ageing with those associated with
304 biofouling. Nevertheless, this pattern corresponds to the progressive increase in chemical
305 ageing accompanied by a more or less intense organic fouling. The β pattern was
306 characterized by spectra with bands related to a relatively intense organic fouling. Finally, the
307 γ pattern was dominated by spectra showing a strong band at 1003 cm^{-1}, indicative of
308 inorganic fouling. The density of the plotted spectra on the PCA decreases beyond the α, β or
309 γ patterns. Between these areas of higher spectra density there were others for which little or
310 no spectrum was projected. For example, no spectrum was projected onto the origin of the
311 axes (zone I). This implied that all the spectra of the collected MP were therefore different
312 from the reference spectrum and none of them can be considered as unaged PS. Zone II
313 corresponded to an area with no point on the factorial map and indicated that it was unlikely
314 that a PS spectrum could have a strong carbonyl band without also having a more or less
315 significant organic fouling. This could mean that chemical ageing and organic fouling
316 processes occur together in the natural environment, but with varying degrees. Zone III
317 appeared between the α and β patterns. This also could mean that when the bands associated
318 with biofouling were very intense, it was more difficult to also have very intense carbonyl
319 bands. Zone IV, visible between the β and γ patterns, was also characterized by a near absence
320 of spectra. This could indicate that spectra with intense bands related to both significant bio
321 and inorganic fouling were more unlikely. It is indeed possible that when the fouling of the
322 surface is important, the MP are more protected from UV rays and age less chemically.
323 Finally, zone V corresponded to an area without a point on the factorial map that can probably
324 be explained by the component loadings. Indeed, since both components were sensitive to the
325 band at 1003 cm^{-1} (PC1 in positive, PC2 in negative), no spectrum presenting the
326 characteristics of an inorganic fouling can be projected into zone V. And as no other band had

significant weight on the negative PC2, no other type of spectrum could be projected below 0 on the y-axis.

The distribution of the spectra on the PCA was different for the PE and PP as they clearly showed a bifid pattern (Fig. 4.b and c). Thus, the α and β branches were well present, but the γ branch, specific to inorganic fouling was absent while it was present on the PCA of the PS spectra. Thus, for these two polymers, inorganic fouling seemed to be rare or very weak. In the case of PE, the average spectrum of the Zone I spectra showed distinct and well-marked, but weak carbonyl bands. Few spectra were found in this zone (0.7%), indicating that most of the PE spectra showed additional bands compared to the unaged PE reference (Fig. 4.b). For the ω region, corresponding to most of the spectra (30.7%), bands associated with moderate biofouling appeared in addition to those of chemical ageing. The average spectrum of the α-pattern was characterized by strong carbonyl bands and less pronounced biofouling-related bands. In contrast, the average spectrum of the β-pattern was characterized by strong biofouling-related bands and weaker carbonyl bands. In the case of PP, the average spectrum of the ω zone indicated low fouling and low chemical ageing (Fig. 4.c). The average spectrum of the α pattern indicated stronger chemical ageing while that of the β pattern indicated strong organic fouling. For these two polymers the interpretations of zones II and III were similar to those of PS. Zone VI implied that inorganic fouling was low for both chemical families of polymers. Caution should be exercised in interpreting these trends. It is possible that chemical ageing and fouling may occur simultaneously or sequentially. For the moment, we have no diagnostic element to distinguish between these two cases. For the bands between 1800 and 1700 cm^{-1}, it is also difficult at this stage to discriminate between the chemical ageing part and the organic fouling part. There is currently a lack of understanding of these trends and new experiments need to be conducted.

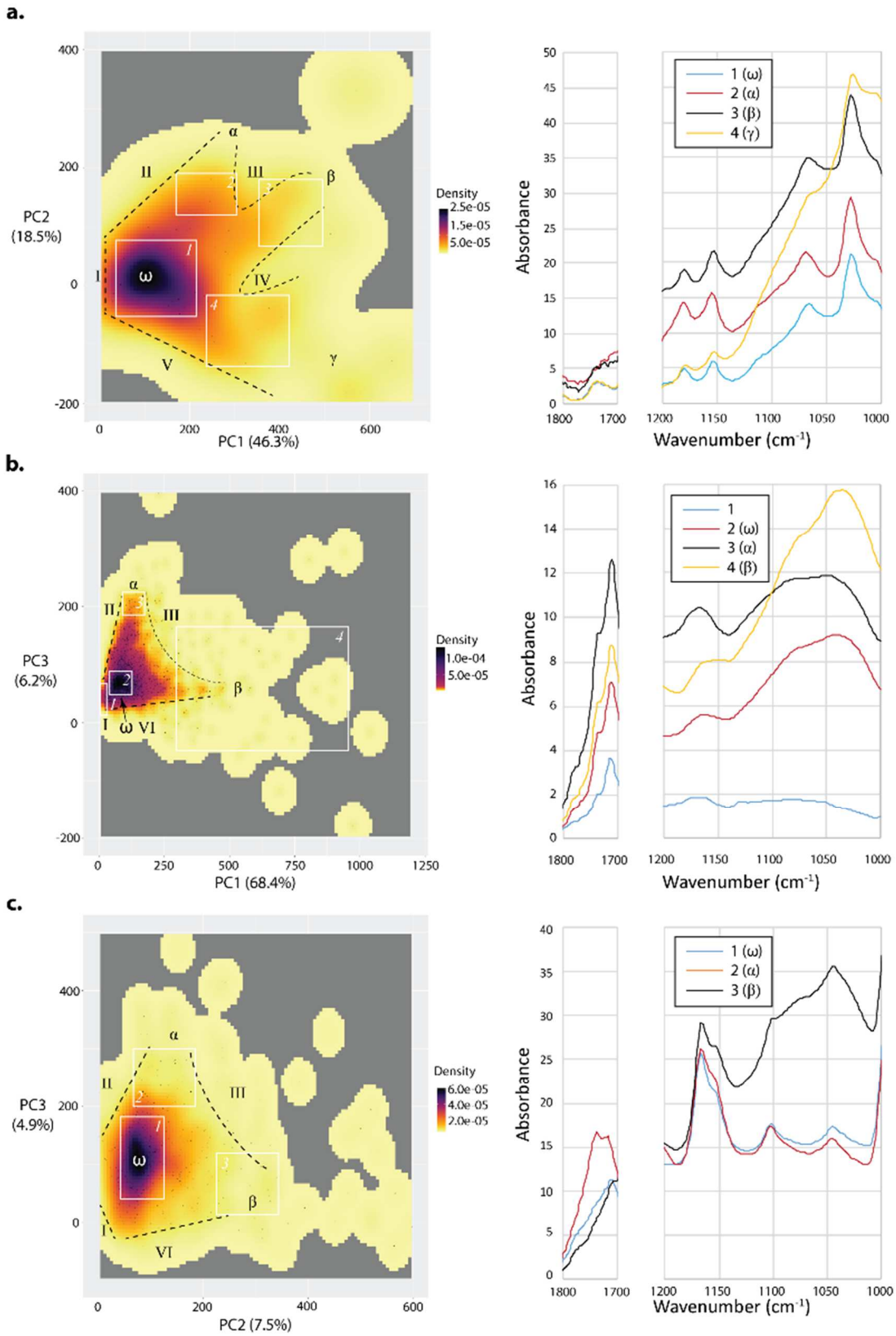
a.
PC2 (18.5%)
PC1 (46.3%)
Density
2.5e-05
1.5e-05
5.0e-05
Absorbance
Wavenumber (cm-1)
1 (ω)
2 (α)
3 (β)
4 (γ)
b.
PC3 (6.2%)
PC1 (68.4%)
Density
1.0e-04
5.0e-05
Absorbance
Wavenumber (cm-1)
1
2 (ω)
3 (α)
4 (β)
c.
PC3 (4.9%)
PC2 (7.5%)
Density
6.0e-05
4.0e-05
2.0e-05
Absorbance
Wavenumber (cm-1)
1 (ω)
2 (α)
3 (β)

351

Fig. 4. Factorial map of poly(styrene) (PS), poly(ethylene) (PE) et poly(propylene) (PP) spectra. a. PS triffid pattern. b. PE biffid pattern. c. PP biffid pattern. See explanation in the text.

3.4. Characterisation of the plastisphere with a fouling index

We propose to use these bands to create an index to describe the fouling of (micro)plastics in the marine environment. For this purpose, the broad band between 1200 and 900 cm^{-1} which peaks show up between 1040 and 1020 cm^{-1} were first considered. This broad band resulted from the overlay of bands at 1070 cm^{-1}, 1045 cm^{-1}, 1003 cm^{-1}. It should be noted that PE does not exhibit a significant band in this frequency range. Since this polymer is the most common in many environmental media and matrices, it was the best candidate for monitoring fouling extent by infrared spectroscopy (Erni-Cassola et al., 2019; Kedzierski et al., 2022; Schwarz et al., 2019). The most common denominator of the PE indices (*i.e.* carbonyl index, hydroxyl index, vinyl index) is generally the intensity of the band at 1470 cm^{-1} (Julienne et al., 2019). Therefore, we proposed a fouling index (FI) that could be calculated as follows (Kedzierski et al., 2022):

$$FI = \frac{I_{1040-1020}}{I_{1480-1460}} \quad (1)$$

With $I_{1040\text{-}1020}$ mainly corresponding to the bands of algal polysaccharides, as well as to a lesser extent to Si-O-Si bonds, and $I_{1480\text{-}1460}$ corresponding to $–CH_2$ scissoring of PE.

Was it possible to refine the monitoring of fouling by resolving inorganic from organic fouling? The band at 1003 cm^{-1} reflecting inorganic fouling and the band at 1045 cm^{-1} reflecting organic fouling were better expressed, and thus appeared to be good candidates. Nevertheless, these two bands showed a significant correlation (r=0.96), implying that these two bands were too spectrally close to each other (Fig. 5). The same applied to the band located at 1070 cm^{-1} which also correlated closely with the other two.

Fig. 5. Parametric correlation coefficient (Pearson's *r*) of different spectral bands. The absorbance values at 1003, 1045 and 1070 cm^{-1} are highly correlated probably due to the overlap of these bands.

The silicate bands at 3678, 800 and 665 cm^{-1} were too weakly expressed or readable on the spectra to be useful. Thus, an index of inorganic fouling did not seem to be possible for the moment without using, for example, a Gaussian peak fitting method. For biofouling, on the other hand, the band at 1637 cm^{-1} (ν(C=O) , protein) was very interesting and allowed us to propose the following organic fouling index:

$$F_oI = \frac{I_{1647-1627}}{I_{1480-1460}} \qquad (2)$$

With $I_{1647\text{-}1627}$ corresponding to amide I band of algal proteins.

The ranking of the PE MP spectra according to the importance of F_oI illustrated the increase of organic fouling (Fig. 6.a): for 59% of the PE spectra the F_oI index was below 0.2. In this case, the fouling was visually characterized by faint bands indicating a weak organic fouling. Between 0.2 and 0.4 (32% of the PE spectra), bands were clearly visible between 1300 and 900 cm^{-1} (i.e. bands attributed to the stretching of C=O bonds from algal proteins).

Approximately 9% of the spectra showed a F_oI greater than 0.4, indicating significant organic fouling. The fact that the majority of MP have a low FoI could be an indication that these MP had been present for a relatively "short time" in the natural environment. This would suggest a relatively short drift time of MP on the ocean surface, which could be of the order of a few dozen days according to experimental data (Fazey and Ryan, 2016). This short time scale (a few weeks) also agrees with an average residence time of plastics in the Mediterranean Sea between 7 and 90 days (Baudena et al., 2022; Liubartseva et al., 2018; Pedrotti et al., 2022). Another possibility is that the environmental conditions were globally not favorable to biofouling. The sampling season could for example have an impact, the spring-summer period being favourable to organic fouling, the autumn-winter less so. Thus, the application of the FI index on PE samples showed that this index was significantly higher in June than in September-October, thus showing a probable sensitivity to seasonality (Kedzierski et al., 2022). However, in our case, samples were mostly sampled in summer, so from this particular point environmental conditions seem quite favorable to fouling. Another very interesting hypothesis can also be formulated: it is possible that the more intensively a microplastic is biofouled (i.e. with a high F_oI index), the greater the probability that it will sediment (Fazey and Ryan, 2016; Kooi et al., 2017, 2016; Lobelle and Cunliffe, 2011). Thus, it is possible that the two proposed indices directly reflect the fouling state of the plastic and indirectly its ability to remain on the water surface. However, further investigations are needed to verify this proposition.

Is it possible to determine the nature of the plastisphere present on the polymer surface by the way of the FTIR spectrum? For example, in the case of the TM0048A3 sample, a PE pellet with a moderate F_oI (0.23), it was possible to observe on its surface areas of green colour (Fig. 6.b). SEM observation revealed the presence of diatoms (*Bacillariophyta*) that had largely colonised the infractuosities (Fig. 6.c). Analysis of the FTIR spectrum showed that in addition

417 to the band at 1045 cm^{-1}, a characteristic shoulder is visible at 1100-1060 cm^{-1}, reflecting the
418 presence of diatom frustule silica (fig. 6.d) (Murdock and Wetzel, 2009). This diatom
419 fingerprint was visible on a very large number of PE spectra. Thus, from the point of view of
420 FTIR spectra, diatoms could be a good marker of the plastisphere. The study of microalgae by
421 FTIR is well established in the literature (Murdock and Wetzel, 2009). Thus, this scientific
422 literature has shown that it is possible to use FTIR spectra determine the nature of the
423 microalgae (Marcilla et al., 2009; Murdock and Wetzel, 2009), their biomass (Stehfest et al.,
424 2005; Sudhakar and Premalatha, 2015) or the biological responses of the microalgae to their
425 environment (Giordano et al., 2001; Murdock and Wetzel, 2009). In the case of microplastic
426 pollution, diatoms are sensitive to certain additives (Wang et al., 2020). In the slightly
427 different case of an aquatic matrix contaminated with a micropollutant, the toxicity to diatoms
428 may be minimised by the presence of the microplastic (Guo et al., 2020; Hao et al., 2022).
429 The fact that the impact may be expressed in terms of variations in lipid accumulation (Guo et
430 al., 2020), suggests that these variations may also be observed in the FTIR spectra,
431 particularly between 2968 and 2861 cm^{-1}.The question is therefore whether this kind of
432 information could also be exploited from microplastic FTIR spectra. These organisms are also
433 likely to accelerate the transfer of microplastics from the ocean surface to the seabed through
434 their ability to form aggregates (Long et al., 2015). It would therefore be interesting to verify
435 whether there is a link between the proposed indices and their buoyancy. Finally, FTIR
436 spectra of microplastics do not only contain information on microalges and recently it has
437 been shown that information on fungal species can be extracted from the study of these
438 spectra (Battulga et al., 2022). This again suggests that the amount of information that can be
439 derived from FTIR spectra of microplastics is probably currently under-exploited.

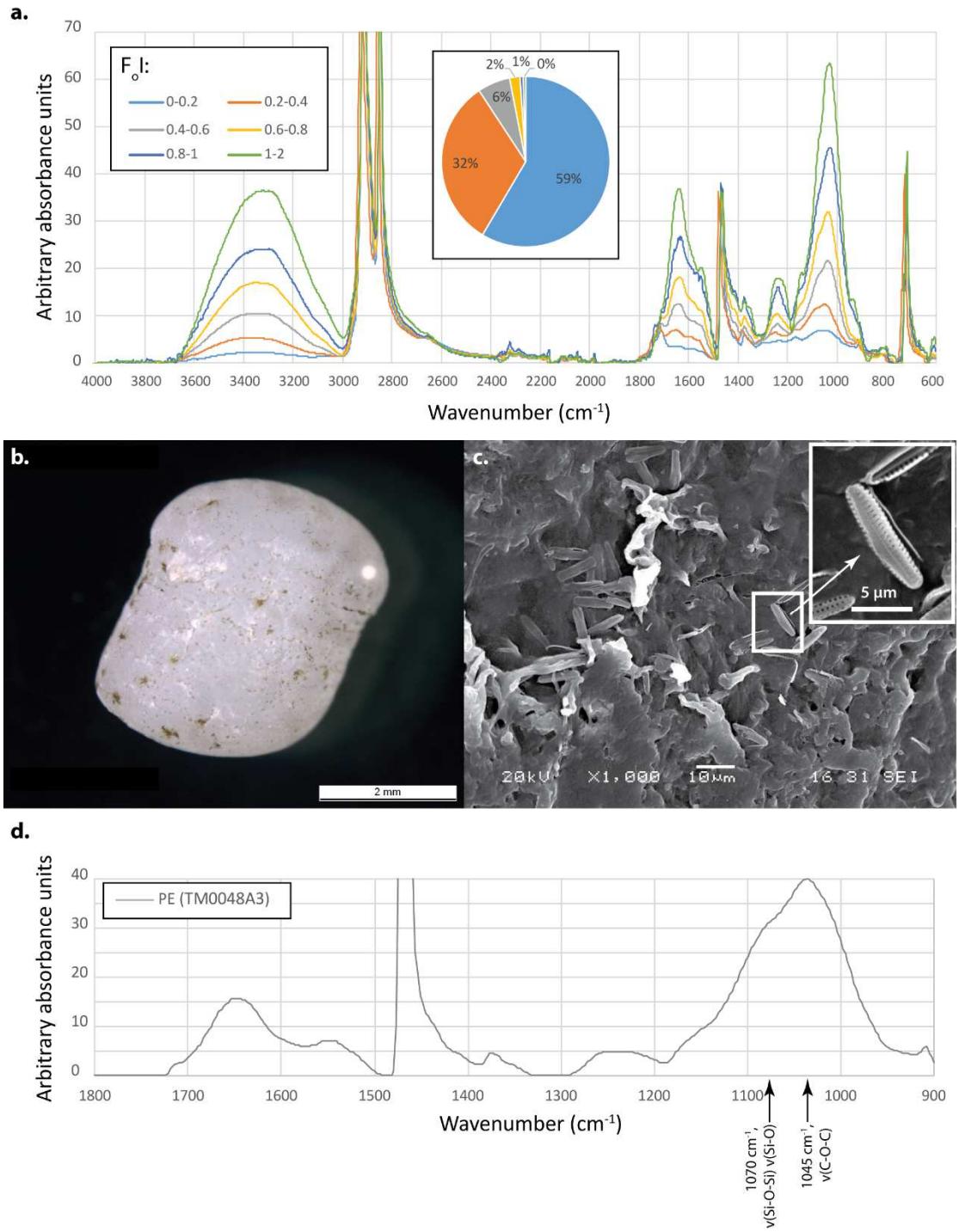

440

441 Fig. 6. ATR-FTIR study of the plastisphere. a. Average PE spectra for different FoI index
442 (biofouling index) ranges and percent of PE spectra in these different classes. b. Photograph
443 of TM0048A3. c. SEM photograph of the surface of the sample TM0048A3. Diatoms were
444 clearly visible. d. Infrared spectrum of TM0048A3. The two bands of the spectrum could be
445 the chemical translation of the presence of diatoms.

4. Conclusions

This study showed that the spectral variability of PE, PP and PS MP collected in the Mediterranean Sea was mainly related to three processes: chemical ageing, organic fouling and inorganic fouling. In most cases, these processes lead to relatively limited changes in the spectra, and only a small proportion of the spectra showed advanced changes. Among the identified processes, inorganic fouling was only clearly evident for PS spectra and not for those of PE and PP. This observation tends to show that these processes probably differ from one polymer family to another due to surface affinities. Furthermore, the different patterns observed within the spectra of the same chemical family of plastics could be an indication that the different processes at work could be more or less uncorrelated. The precise mechanisms behind these intra- and inter-chemical group variations remain to be explained and are of utmost interest to better understand the fate of MPs in oceans.

This work has led to the proposal of two new indices: the fouling index (FI) and the organic fouling index (FoI). These two indices provide important and hitherto unexploited information, and raise the question of their use to monitor the intensity of (bio)fouling on the surface of (micro)plastics. The advanced analysis of spectra must also provide information on the nature of the plastisphere (*eg.* diatoms on PE).

Our study focused on most abundant types of polymers, from samples taken from the surface of the Mediterranean Sea. It is therefore relevant to ask the question of the possibility of generalizing these results (i.e. to other polymers, other oceans, other environmental matrices). The re-exploitation of existing FTIR spectra databases of MP would enable to rapidly provide answers to these questions.

ACKNOWLEDGMENTS

We thank the commitment of the following institutions, persons and sponsors: CNRS, UPMC, LOV, Genoscope/CEA, the Tara Expeditions Foundation and its founders: agnès b.®, Etienne Bourgois, Romain Troublé, the Veolia Environment Foundation, Lorient Agglomeration, Serge Ferrari, the Foundation Prince Albert II de Monaco, IDEC, the "Tara" schooner and teams. We thank MERCATOR-CORIOLIS and ACRI-ST for providing daily satellite data during the expedition. We are also grateful to the French Ministry of Foreign Affairs for supporting the expedition and to the countries that graciously granted sampling permission. We would like to thank Marie Emmanuelle Kerros and Maryvonne Henry for their help in the analysis of plastics. Finally, we thank Olivier Sire for his proofreading and useful comments.

REFERENCES

Amaral-Zettler, L.A., Zettler, E.R., Mincer, T.J., 2020. Ecology of the plastisphere. Nat. Rev. Microbiol. 18, 139–151. https://doi.org/10.1038/s41579-019-0308-0

Anbalagan, G., Prabakaran, A., Gunasekaran, S., 2010. Spectroscopic characterization of indian standard sand. J. Appl. Spectrosc. 77, 86–94. https://doi.org/10.1007/s10812-010-9297-5

Andrady, A.L., 2017. The plastic in microplastics: A review. Mar. Pollut. Bull. 119, 12–22. https://doi.org/https://doi.org/10.1016/j.marpolbul.2017.01.082

Andrady, A.L., 2011. Microplastics in the marine environment. Mar. Pollut. Bull. 62, 1596–1605. https://doi.org/10.1016/j.marpolbul.2011.05.030

Andrady, A.L., Pegram, J.E., 1991. Weathering of polystyrene foam on exposure in air and in seawater. J. Appl. Polym. Sci. 42, 1589–1596. https://doi.org/doi:10.1002/app.1991.070420612

Avio, C.G., Gorbi, S., Regoli, F., 2017. Plastics and microplastics in the oceans: From emerging pollutants to emerged threat. Mar. Environ. Res. 128, 2–11.

493 https://doi.org/https://doi.org/10.1016/j.marenvres.2016.05.012

494 Battulga, B., Kawahigashi, M., Oyuntsetseg, B., 2022. Characterization of biofilms formed on
495 polystyrene microplastics (PS-MPs) on the shore of the Tuul River, Mongolia. Environ.
496 Res. 212, 113329. https://doi.org/https://doi.org/10.1016/j.envres.2022.113329

497 Baudena, A., Ser-Giacomi, E., Jalón-Rojas, I., Galgani, F., Pedrotti, M.L., 2022. The
498 streaming of plastic in the Mediterranean Sea. Nat. Commun. 13, 2981.
499 https://doi.org/10.1038/s41467-022-30572-5

500 Chércoles Asensio, R., San Andrés Moya, M., de la Roja, J.M., Gómez, M., 2009. Analytical
501 characterization of polymers used in conservation and restoration by ATR-FTIR
502 spectroscopy. Anal. Bioanal. Chem. 395, 2081–2096. https://doi.org/10.1007/s00216-
503 009-3201-2

504 Cózar, A., Martí, E., Duarte, C.M., García-de-Lomas, J., van Sebille, E., Ballatore, T.J.,
505 Eguíluz, V.M., González-Gordillo, J.I., Pedrotti, M.L., Echevarría, F., Troublè, R.,
506 Irigoien, X., 2017. The Arctic Ocean as a dead end for floating plastics in the North
507 Atlantic branch of the Thermohaline Circulation. Sci. Adv. 3.
508 https://doi.org/10.1126/sciadv.1600582

509 Dean, A.P., Sigee, D.C., Estrada, B., Pittman, J.K., 2010. Using FTIR spectroscopy for rapid
510 determination of lipid accumulation in response to nitrogen limitation in freshwater
511 microalgae. Bioresour. Technol. 101, 4499–4507.
512 https://doi.org/https://doi.org/10.1016/j.biortech.2010.01.065

513 Dehaut, A., Cassone, A.-L., Frère, L., Hermabessiere, L., Himber, C., Rinnert, E., Rivière, G.,
514 Lambert, C., Soudant, P., Huvet, A., Duflos, G., Paul-Pont, I., 2016. Microplastics in
515 seafood: Benchmark protocol for their extraction and characterization. Environ. Pollut.
516 215, 223–233. https://doi.org/http://dx.doi.org/10.1016/j.envpol.2016.05.018

517 Dokmai, V., Sinthiptharakoon, K., Phuthong, W., Pavarajarn, V., 2021. Anisotropic
518 robustness of talc particles after surface modifications probed by atomic force
519 microscopy force spectroscopy. Particuology.
520 https://doi.org/https://doi.org/10.1016/j.partic.2021.04.008

521 Doyen, P., Hermabessiere, L., Dehaut, A., Himber, C., Decodts, M., Degraeve, T., Delord, L.,
522 Gaboriaud, M., Moné, P., Sacco, J., Tavernier, E., Grard, T., Duflos, G., 2019.
523 Occurrence and identification of microplastics in beach sediments from the Hauts-de-
524 France region. Environ. Sci. Pollut. Res. 26, 28010–28021.
525 https://doi.org/10.1007/s11356-019-06027-8

526 Erni-Cassola, G., Zadjelovic, V., Gibson, M.I., Christie-Oleza, J.A., 2019. Distribution of
527 plastic polymer types in the marine environment; A meta-analysis. J. Hazard. Mater. 369,
528 691–698. https://doi.org/https://doi.org/10.1016/j.jhazmat.2019.02.067

529 Fazey, F.M.C., Ryan, P.G., 2016. Biofouling on buoyant marine plastics: An experimental
530 study into the effect of size on surface longevity. Environ. Pollut. 210, 354–360.
531 https://doi.org/http://dx.doi.org/10.1016/j.envpol.2016.01.026

532 Fernández-González, V., Andrade-Garda, J.M., López-Mahía, P., Muniategui-Lorenzo, S.,
533 2021. Impact of weathering on the chemical identification of microplastics from usual
534 packaging polymers in the marine environment. Anal. Chim. Acta 1142, 179–188.
535 https://doi.org/https://doi.org/10.1016/j.aca.2020.11.002

536 Gewert, B., Ogonowski, M., Barth, A., MacLeod, M., 2017. Abundance and composition of
537 near surface microplastics and plastic debris in the Stockholm Archipelago, Baltic Sea.
538 Mar. Pollut. Bull. In Press.
539 https://doi.org/https://doi.org/10.1016/j.marpolbul.2017.04.062

540 Giordano, M., Kansiz, M., Heraud, P., Beardall, J., Wood, B., McNaughton, D., 2001.

541 FOURIER TRANSFORM INFRARED SPECTROSCOPY AS A NOVEL TOOL TO
542 INVESTIGATE CHANGES IN INTRACELLULAR MACROMOLECULAR POOLS
543 IN THE MARINE MICROALGA CHAETOCEROS MUELLERII
544 (BACILLARIOPHYCEAE). J. Phycol. 37, 271–279.
545 https://doi.org/https://doi.org/10.1046/j.1529-8817.2001.037002271.x

546 Guo, Y., Ma, W., Li, J., Liu, W., Qi, P., Ye, Y., Guo, B., Zhang, J., Qu, C., 2020. Effects of
547 microplastics on growth, phenanthrene stress, and lipid accumulation in a diatom,
548 Phaeodactylum tricornutum. Environ. Pollut. 257, 113628.
549 https://doi.org/https://doi.org/10.1016/j.envpol.2019.113628

550 Hammer, Ø., Harper, D.A.T., Ryan, P.D., 2001. Past: Paleontological Statistics Software
551 Package for Education and Data Analysis . Palaeontol. Electron. 4, 9.

552 Hao, B., Wu, H., Zhang, S., He, B., 2022. Individual and combined toxicity of microplastics
553 and diuron differs between freshwater and marine diatoms. Sci. Total Environ. 853,
554 158334. https://doi.org/https://doi.org/10.1016/j.scitotenv.2022.158334

555 Hüffer, T., Weniger, A.-K., Hofmann, T., 2018. Sorption of organic compounds by aged
556 polystyrene microplastic particles. Environ. Pollut. 236, 218–225.
557 https://doi.org/https://doi.org/10.1016/j.envpol.2018.01.022

558 Huo, Y., Dijkstra, F.A., Possell, M., Singh, B.B.T.-A. in A., 2022. Plastics in soil
559 environments: All things considered. Academic Press.
560 https://doi.org/https://doi.org/10.1016/bs.agron.2022.05.002

561 Imhof, H.K., Sigl, R., Brauer, E., Feyl, S., Giesemann, P., Klink, S., Leupolz, K., Loder,
562 M.G., Loschel, L.A., Missun, J., Muszynski, S., Ramsperger, A.F., Schrank, I., Speck,
563 S., Steibl, S., Trotter, B., Winter, I., Laforsch, C., 2017. Spatial and temporal variation of
564 macro-, meso- and microplastic abundance on a remote coral island of the Maldives,

565 Indian Ocean. Mar. Pollut. Bull. 116, 340–347.
566 https://doi.org/10.1016/j.marpolbul.2017.01.010

567 Julienne, F., Delorme, N., Lagarde, F., 2019. From macroplastics to microplastics: Role of
568 water in the fragmentation of polyethylene. Chemosphere 236, 124409.
569 https://doi.org/https://doi.org/10.1016/j.chemosphere.2019.124409

570 Kedzierski, M., Falcou-Préfol, M., Kerros, M.E., Henry, M., Pedrotti, M.L., Bruzaud, S.,
571 2019a. A machine learning algorithm for high throughput identification of FTIR spectra:
572 Application on microplastics collected in the Mediterranean Sea. Chemosphere 234,
573 242–251. https://doi.org/10.1016/j.chemosphere.2019.05.113

574 Kedzierski, M., Palazot, M., Soccalingame, L., Falcou-Préfol, M., Gorsky, G., Galgani, F.,
575 Bruzaud, S., Pedrotti, M.L., 2022. Chemical composition of microplastics floating on the
576 surface of the Mediterranean Sea. Mar. Pollut. Bull. 174, 113284.
577 https://doi.org/https://doi.org/10.1016/j.marpolbul.2021.113284

578 Kedzierski, M., Villain, J., Falcou-Préfol, M., Kerros, M.E., Henry, M., Pedrotti, M.L.,
579 Bruzaud, S., 2019b. Microplastics in Mediterranean Sea: A protocol to robustly assess
580 contamination characteristics. PLoS One 14, e0212088.
581 https://doi.org/10.1371/journal.pone.0212088

582 Kooi, M., Nes, E.H. van, Scheffer, M., Koelmans, A.A., 2017. Ups and Downs in the Ocean:
583 Effects of Biofouling on Vertical Transport of Microplastics. Environ. Sci. Technol. 51,
584 7963–7971. https://doi.org/10.1021/acs.est.6b04702

585 Kooi, M., Reisser, J., Slat, B., Ferrari, F.F., Schmid, M.S., Cunsolo, S., Brambini, R., Noble,
586 K., Sirks, L.-A., Linders, T.E.W., Schoeneich-Argent, R.I., Koelmans, A.A., 2016. The
587 effect of particle properties on the depth profile of buoyant plastics in the ocean. Sci.
588 Rep. 6, 33882. https://doi.org/10.1038/srep33882

589 Lacerda, A.L. d. F., Rodrigues, L. dos S., van Sebille, E., Rodrigues, F.L., Ribeiro, L., Secchi,
590 E.R., Kessler, F., Proietti, M.C., 2019. Plastics in sea surface waters around the Antarctic
591 Peninsula. Sci. Rep. 9, 3977. https://doi.org/10.1038/s41598-019-40311-4

592 Lafuente, B., Downs, R.T., Yang, H., Stone, N., 2015. 1. The power of databases: The
593 RRUFF project, in: Armbruster, T., Danisi, R.M. (Eds.), . De Gruyter (O), pp. 1–30.
594 https://doi.org/doi:10.1515/9783110417104-003

595 Liland, K.H., 2015. 4S Peak Filling – baseline estimation by iterative mean suppression.
596 MethodsX 2, 135–140. https://doi.org/10.1016/j.mex.2015.02.009

597 Liubartseva, S., Coppini, G., Lecci, R., Clementi, E., 2018. Tracking plastics in the
598 Mediterranean: 2D Lagrangian model. Mar. Pollut. Bull. 129, 151–162.
599 https://doi.org/https://doi.org/10.1016/j.marpolbul.2018.02.019

600 Lobelle, D., Cunliffe, M., 2011. Early microbial biofilm formation on marine plastic debris.
601 Mar. Pollut. Bull. 62, 197–200.
602 https://doi.org/https://doi.org/10.1016/j.marpolbul.2010.10.013

603 Lobo, H., Bonilla, J. V., 2003. Handbook of plastics analysis. Taylor & Francis Group, New
604 York - Basel.

605 Long, M., Moriceau, B., Gallinari, M., Lambert, C., Huvet, A., Raffray, J., Soudant, P., 2015.
606 Interactions between microplastics and phytoplankton aggregates: Impact on their
607 respective fates. Mar. Chem. 175, 39–46. https://doi.org/10.1016/j.marchem.2015.04.003

608 Long, Z., Pan, Z., Wang, W., Ren, J., Yu, X., Lin, L., Lin, H., Chen, H., Jin, X., 2019.
609 Microplastic abundance, characteristics, and removal in wastewater treatment plants in a
610 coastal city of China. Water Res. 155, 255–265.
611 https://doi.org/https://doi.org/10.1016/j.watres.2019.02.028

612 Mailhot, B., Gardette, J.-L., 1992. Polystyrene photooxidation. 1. Identification of the IR-
613 absorbing photoproducts formed at short and long wavelengths. Macromolecules 25,
614 4119–4126.

615 Marcilla, A., Gómez-Siurana, A., Gomis, C., Chápuli, E., Catalá, M.C., Valdés, F.J., 2009.
616 Characterization of microalgal species through TGA/FTIR analysis: Application to
617 nannochloropsis sp. Thermochim. Acta 484, 41–47.
618 https://doi.org/https://doi.org/10.1016/j.tca.2008.12.005

619 Morgado, V., Gomes, L., Bettencourt da Silva, R., Palma, C., 2021. Validated spreadsheet for
620 the identification of PE, PET, PP and PS microplastics by micro-ATR-FTIR spectra with
621 known uncertainty. Talanta 122624.
622 https://doi.org/https://doi.org/10.1016/j.talanta.2021.122624

623 Murdock, J.N., Wetzel, D.L., 2009. FT-IR Microspectroscopy Enhances Biological and
624 Ecological Analysis of Algae. Appl. Spectrosc. Rev. 44, 335–361.
625 https://doi.org/10.1080/05704920902907440

626 Napper, I.E., Davies, B.F.R., Clifford, H., Elvin, S., Koldewey, H.J., Mayewski, P.A., Miner,
627 K.R., Potocki, M., Elmore, A.C., Gajurel, A.P., Thompson, R.C., 2020. Reaching New
628 Heights in Plastic Pollution—Preliminary Findings of Microplastics on Mount Everest.
629 One Earth 3, 621–630. https://doi.org/https://doi.org/10.1016/j.oneear.2020.10.020

630 Pedrotti, M.L., Lombard, F., Baudena, A., Galgani, F., Elineau, A., Petit, S., Henry, M.,
631 Troublé, R., Reverdin, G., Ser-Giacomi, E., Kedzierski, M., Boss, E., Gorsky, G., 2022.
632 An integrative assessment of the plastic debris load in the Mediterranean Sea. Sci. Total
633 Environ. 838, 155958. https://doi.org/https://doi.org/10.1016/j.scitotenv.2022.155958

634 Prata, J.C., da Costa, J.P., Duarte, A.C., Rocha-Santos, T., 2019. Methods for sampling and
635 detection of microplastics in water and sediment: A critical review. TrAC - Trends Anal.

636 Chem. 110, 150–159. https://doi.org/10.1016/j.trac.2018.10.029

637 Primpke, S., Fischer, M., Lorenz, C., Gerdts, G., Scholz-Böttcher, B.M., 2020. Comparison of
638 pyrolysis gas chromatography/mass spectrometry and hyperspectral FTIR imaging
639 spectroscopy for the analysis of microplastics. Anal. Bioanal. Chem.
640 https://doi.org/10.1007/s00216-020-02979-w

641 Primpke, S., Wirth, M., Lorenz, C., Gerdts, G., 2018. Reference database design for the
642 automated analysis of microplastic samples based on Fourier transform infrared (FTIR)
643 spectroscopy. Anal. Bioanal. Chem. 410, 5131–5141. https://doi.org/10.1007/s00216-
644 018-1156-x

645 Quilès, F., Humbert, F., Delille, A., 2010. Analysis of changes in attenuated total reflection
646 FTIR fingerprints of Pseudomonas fluorescens from planktonic state to nascent biofilm
647 state. Spectrochim. Acta Part A Mol. Biomol. Spectrosc. 75, 610–616.
648 https://doi.org/https://doi.org/10.1016/j.saa.2009.11.026

649 Ramamoorthy, R., Vanitha, S., Krishnadev, P., Paramanantham, M., 2021. Synthesis and
650 characterization of phyto mediated talc-based nanocomposite by wet chemical reduction
651 method. Mater. Today Proc. https://doi.org/https://doi.org/10.1016/j.matpr.2021.03.582

652 Ripley, B.D., 1996. Pattern recognition and neural networks. Cambridge University Press,
653 Cambridge ; New York.

654 Scherer, C., Weber, A., Stock, F., Vurusic, S., Egerci, H., Kochleus, C., Arendt, N., Foeldi,
655 C., Dierkes, G., Wagner, M., Brennholt, N., Reifferscheid, G., 2020. Comparative
656 assessment of microplastics in water and sediment of a large European river. Sci. Total
657 Environ. 738, 139866. https://doi.org/https://doi.org/10.1016/j.scitotenv.2020.139866

658 Schmitt, J., Nivens, D., White, D.C., Flemming, H.-C., 1995. Changes of biofilm properties in

response to sorbed substances - an FTIR-ATR study. Water Sci. Technol. 32, 149–155. https://doi.org/https://doi.org/10.1016/0273-1223(96)00019-4

Schröder, E., Müller, G., Arndt, K.-F., 1989. Polymer Characterization. De Gruyter.

Schroeder, P., 2002. Infrared spectroscopy in clay science. Teach. Clay Sci. 11.

Schwarz, A., Ligthart, T., Boukris, E., Van Harmelen, T., 2019. Sources, transport, and accumulation of different types of plastic litter in aquatic environments: A review study ☆, Marine Pollution Bulletin. https://doi.org/10.1016/j.marpolbul.2019.04.029

Socrates, G., 2004. Infrared and Raman Characteristic Group Frequencies: Tables and Charts, 3rd ed. John Wiley and Sons.

Stehfest, K., Toepel, J., Wilhelm, C., 2005. The application of micro-FTIR spectroscopy to analyze nutrient stress-related changes in biomass composition of phytoplankton algae. Plant Physiol. Biochem. 43, 717–726. https://doi.org/https://doi.org/10.1016/j.plaphy.2005.07.001

Sudhakar, K., Premalatha, M., 2015. Characterization of Micro Algal Biomass Through FTIR/TGA /CHN Analysis: Application to Scenedesmus sp. Energy Sources, Part A Recover. Util. Environ. Eff. 37, 2330–2337. https://doi.org/10.1080/15567036.2013.825661

Syranidou, E., Karkanorachaki, K., Amorotti, F., Franchini, M., Repouskou, E., Kaliva, M., Vamvakaki, M., Kolvenbach, B., Fava, F., Corvini, P.F.-X., Kalogerakis, N., 2017. Biodegradation of weathered polystyrene films in seawater microcosms. Sci. Rep. 7, 17991. https://doi.org/10.1038/s41598-017-18366-y

The R Core Team, 2019. R: A Language and Environment forStatistical Computing.

Venables, W.N., Ripley, B.D., Venables, W.N., 2002. Modern applied statistics with S, 4th

ed, Statistics and computing. Springer, New York.

Wakkaf, T., El Zrelli, R., Yacoubi, L., Kedzierski, M., Lin, Y.-J., Mansour, L., Bruzaud, S., Rabaoui, L., 2022. Seasonal patterns of microplastics in surface sediments of a Mediterranean lagoon heavily impacted by human activities (Bizerte lagoon, Northern Tunisia). Environ. Sci. Pollut. Res. https://doi.org/10.1007/s11356-022-21129-6

Wang, J., Peng, J., Tan, Z., Gao, Y., Zhan, Z., Chen, Q., Cai, L., 2017. Microplastics in the surface sediments from the Beijiang River littoral zone: Composition, abundance, surface textures and interaction with heavy metals. Chemosphere 171, 248–258. https://doi.org/10.1016/j.chemosphere.2016.12.074

Wang, S., Wang, Y., Liang, Y., Cao, W., Sun, C., Ju, P., Zheng, L., 2020. The interactions between microplastic polyvinyl chloride and marine diatoms: Physiological, morphological, and growth effects. Ecotoxicol. Environ. Saf. 203, 111000. https://doi.org/https://doi.org/10.1016/j.ecoenv.2020.111000

Yagoubi, W., Abdelhafidi, A., Sebaa, M., Chabira, S.F., 2015. Identification of carbonyl species of weathered LDPE films by curve fitting and derivative analysis of IR spectra. Polym. Test. 44, 37–48. https://doi.org/https://doi.org/10.1016/j.polymertesting.2015.03.008

Yi, H., Zhao, Y., Liu, Y., Wang, W., Song, S., Liu, C., Li, H., Zhan, W., Liu, X., 2019. A novel method for surface wettability modification of talc through thermal treatment. Appl. Clay Sci. 176, 21–28. https://doi.org/https://doi.org/10.1016/j.clay.2019.04.023

Zhang, K., Hamidian, A.H., Tubić, A., Zhang, Y., Fang, J.K.H., Wu, C., Lam, P.K.S., 2021. Understanding plastic degradation and microplastic formation in the environment: A review. Environ. Pollut. 274, 116554. https://doi.org/https://doi.org/10.1016/j.envpol.2021.116554

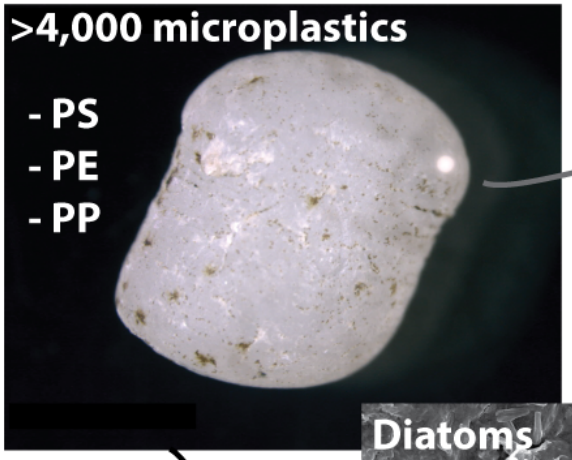

FTIR

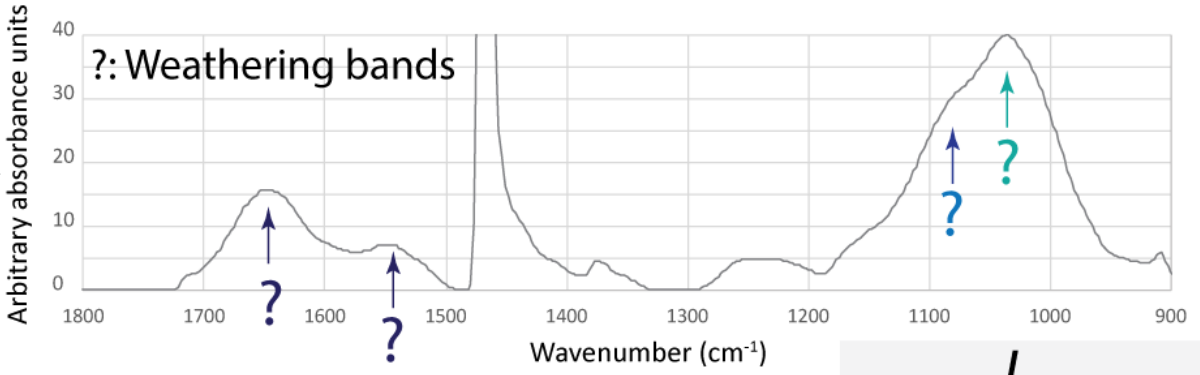

SEM

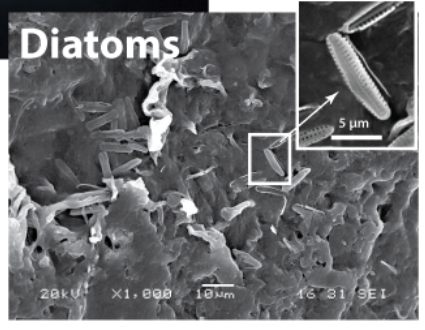

Interpretations

- Algal proteins
- Si–O–Si bonds
- Algal polysaccharides

PE: Fouling indexes

$$FI = \frac{I_{1040\text{-}1020}}{I_{1480\text{-}1460}}$$

$$FoI = \frac{I_{1647\text{-}1627}}{I_{1480\text{-}1460}}$$